Available online at www.sciencedirect.com

SciVerse ScienceDirect

journal homepage: www.elsevier.com/locate/he

Effect of preparation method on the properties of nanostructured gadolinia-doped ceria materials for IT-SOFCs

Fernando F. Muñoz [a], *A. Gabriela Leyva* [b,c], *Richard T. Baker* [d], *Rodolfo O. Fuentes* [a,b,*]

[a] CINSO, UNIDEF (CONICET-MINDEF), J.B. de La Salle 4397, 1603 Villa Martelli, Buenos Aires, Argentina
[b] Gerencia de Investigación y Aplicaciones, CAC, Comisión Nacional de Energía Atómica, Av. Gral. Paz 1499, (1650) San Martín, Buenos Aires, Argentina
[c] Escuela de Ciencia y Tecnología, Universidad Nacional de San Martín, Av. Gral. Paz 1499, (1650) San Martín, Buenos Aires, Argentina
[d] EaStChem, School of Chemistry, University of St. Andrews, North Haugh, St. Andrews, Fife, KY16 9ST, United Kingdom

ARTICLE INFO

Article history:
Received 26 August 2011
Accepted 13 December 2011
Available online 5 January 2012

Keywords:
Solid oxide fuel cells
Nanostructured ceria–gadolinia solid solutions
HRTEM
X-ray powder diffraction
X-ray absorption spectroscopy

ABSTRACT

In order to obtain different morphologies, nanostructured $Gd_{0.1}Ce_{0.9}O_{1.95}$ (GDC10) and $Gd_{0.2}Ce_{0.8}O_{1.90}$ (GDC20) were synthesized using three different chemical methods: reverse microemulsion (RM), cation complexation (CC) and template-filling (TF). The resulting materials were characterized by synchrotron radiation X-ray diffraction (SR-XRD), by X-ray absorption near-edge spectroscopy (XANES) and by scanning and high resolution transmission electron microscopy (SEM and HRTEM). All nanostructured mixed oxides were found to have a cubic crystal phase (*Fm3m* space group) with an average crystallite sizes ranging from 9.6 to 13.2 nm. Tubular nanostructured GDC10 obtained using a template-filling method exhibited the largest specific surface area (97 $m^2\ g^{-1}$) while the lowest values were obtained using the cation complexation method (23 $m^2\ g^{-1}$). XANES results indicated that the extent of reduction of these materials was small. Nevertheless, the Ce^{3+} ion was detected. Preliminary catalytic studies showed that the tubular nanostructured (TF) GDC10 samples exhibited better catalytic activity for CH_4 oxidation than the CC and RM nanopowders of the same chemical composition.

1. Introduction

Ceria (CeO_2) can be doped with aliovalent cations, for example, from the rare earth oxides (Y_2O_3, Gd_2O_3, Sm_2O_3, Nd_2O_3, etc.), to form solid solutions in which vacancies are introduced in the anion sub-lattice as charge-compensating defects. The oxygen ion conductivity of gadolinia-doped ceria (GDC) solid solutions, typically with 10–20% substitution of Ce by Gd, is one of the highest in this class of solid electrolytes [1,2]. For this reason, it is one of the ceria-based solid solutions proposed for intermediate temperature application of SOFCs [3,4]. However, one of the main drawbacks of ceria-based materials is that high temperatures are required to sinter the materials to form dense bodies. To address this problem, different routes for the preparation of ultra-fine powders by both physical and chemical methods have been proposed [5,6]. Such ultra-fine powders are expected to aid sintering and help to bring down the sintering temperature.

A further limitation on GDC and related materials is that, in reducing atmospheres, the presence of both ionic and electronic charge carriers gives rise to mixed (ionic and

* *Corresponding author*. CINSO, UNIDEF (CONICET-MINDEF), J.B. de La Salle 4397, 1603 Villa Martelli, Buenos Aires, Argentina.
E-mail address: rofuentes@conicet.gov.ar (R.O. Fuentes).
0360-3199/$ – see front matter
doi:10.1016/j.ijhydene.2011.12.094

electronic) conducting behavior. This is a difficulty for the application of GDC in SOFC electrolytes – where electronic conductivity would give rise to an internal short circuit of the electrolyte – but would be an advantage for the use of GDC in anodes for IT-SOFCs. Several studies in this area have been reported, especially on the use of GDC as a catalyst support. For this application in particular, it is necessary to obtain materials with large specific surface area (SSA) and high porosity [7–9].

As is mentioned above, for application both as an electrolyte and in the anode it is important to obtain ultra-fine powders. Several chemical routes have been proposed to reach this goal. In general, chemical techniques have the advantage over conventional techniques of yielding high purity, homogeneous and ultra-fine powders of GDC. The synthesis of GDC nanopowders by various wet chemical routes, such as co-precipitation, cation complexation and the combustion routes has been reported [10–12].

We recently reported the preparation by the template-filling synthesis method of nanostructures of Ce-based mixed oxides with tubular morphology [13,14]. Such nanostructures have high specific surface areas (SSAs) that would be expected to lead to high activities, good atomic efficiencies and rapid response to changing conditions in catalyst systems.

In the present work, we compare the properties of nanostructured $Gd_{0.1}Ce_{0.9}O_{1.95}$ (GDC10) and $Gd_{0.2}Ce_{0.8}O_{1.90}$ (GDC20) synthesized by following three different chemical methods to yield different morphologies. Reverse microemulsion, cation complexation and template-filling methods were employed. The resulting materials were characterized by employing synchrotron radiation X-ray diffraction (SR-XRD), X-ray absorption near-edge spectroscopy (XANES) and high resolution transmission electron microscopy (HRTEM). Finally, preliminary tests of the catalytic activity for CH_4 combustion were performed on these nanostructured materials.

2. Experimental

2.1. Synthesis of nanostructured gadolinia-doped ceria solid solutions

Three different methods were used to obtain nanostructured $Gd_{0.1}Ce_{0.9}O_{1.95}$ (GDC10) and $Gd_{0.2}Ce_{0.8}O_{1.90}$ (GDC20) mixed oxide. $Ce(NO_3)_3.6H_2O$ (99.99%, Alfa Aesar) and $Gd(NO_3)_3\cdot 6H_2O$ (99.9%, Acros) were employed as precursors. Each nitrate was dissolved in pure H_2O separately and then the solutions were mixed to obtain a nitrate solution with a molar Ce:Gd stoichiometry appropriate for the preparation of GDC10 and GDC20. Fig. 1 presents the flow diagrams of the three methods employed in this work.

2.1.1. Cation complexation method (CC)

Different amounts of citric acid (99.5%-Merck) were dissolved in d.i. water and this was added to the cation nitrate solution. The molar ratio of total oxide (TO) to citric acid (CA) was 1:2. After homogenization of this solution, the temperature was raised to 80 °C, and the solution maintained under stirring to remove excess water and to convert it to a transparent gel. While raising the temperature, the solution became more viscous with evolution of foam, and finally it gelled without any visible precipitation or turbidity. During the dwell at 80 °C there was an increase in viscosity and simultaneous elimination of water and NO_2. The initial thermal

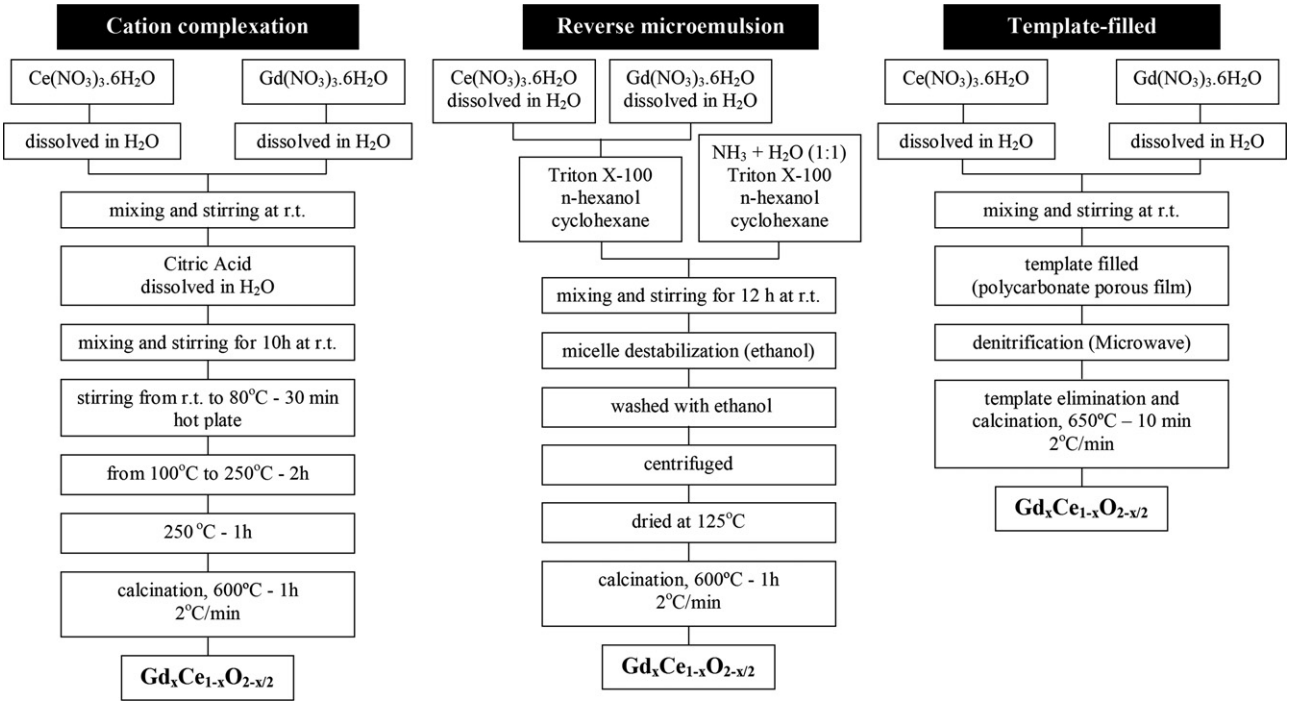

Fig. 1 – Flowchart illustrating the three different synthetic routes used to obtain nanocrystalline GDC solid solutions.

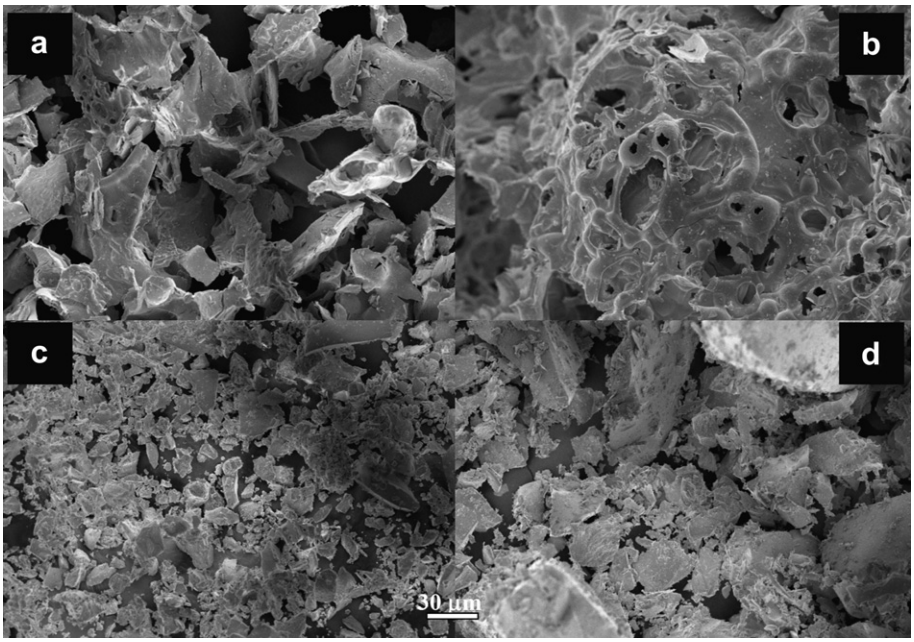

Fig. 2 – SEM images of (a) GDC10-CC, (b) GDC20-CC (c) GDC10-RM and (d) GDC20-RM.

decomposition of the precursor was carried out at 250 °C for 1 h. The resulting ash-like material was calcined at 600 °C for 1 h in air [15,16].

2.1.2. Reverse microemulsion method (RM)

For each preparation, two microemulsions were prepared by mixing in each case the surfactant Triton X-100 (octylphenol ethoxylate) (AppliChem), n-hexanol (Tedia), and cyclohexane (Tedia), in the volumetric ratio 1:1.3:2.2 respectively. The volume of surfactant was 25 ml. To each microemulsion, 10 ml of aqueous solution was added (resulting in a *w/o* ratio of 1:1.09) under continuous, heavy stirring: in one case the cation nitrate solution (solution A); in the other case, concentrated NH_3 (Merck, diluted by half) (solution B). Each resulting microemulsion was perfectly clear (the one containing the Gd and Ce cations exhibited a moderately intense yellow color) and without any sign of turbidity, showing the stability of the microemulsion so obtained. Both solutions were left to stabilize under stirring for 45 min. Solution B was then added dropwise to solution A, once again under heavy

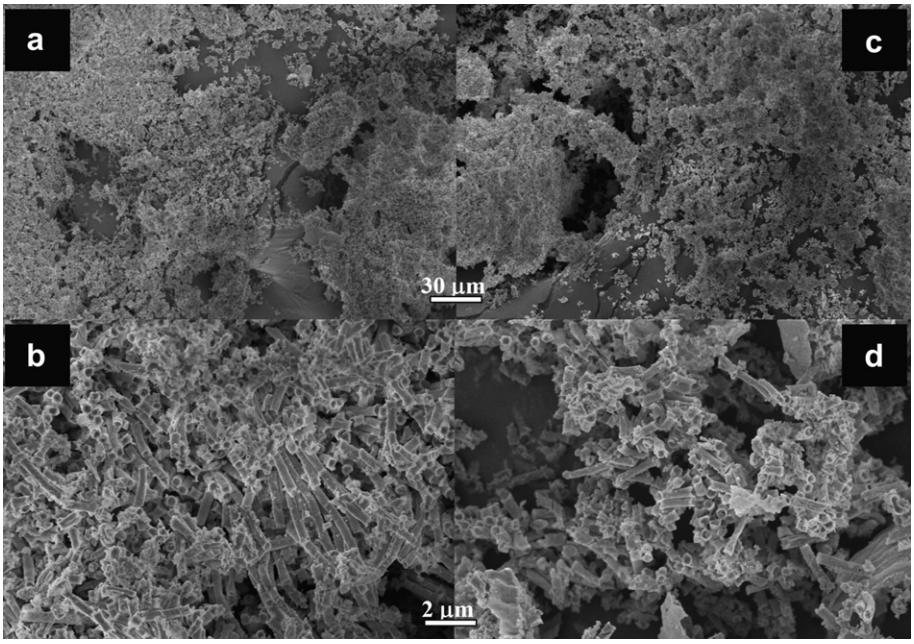

Fig. 3 – SEM images of (a) and (b) GDC10-TF; (c) and (d) GDC20-TF.

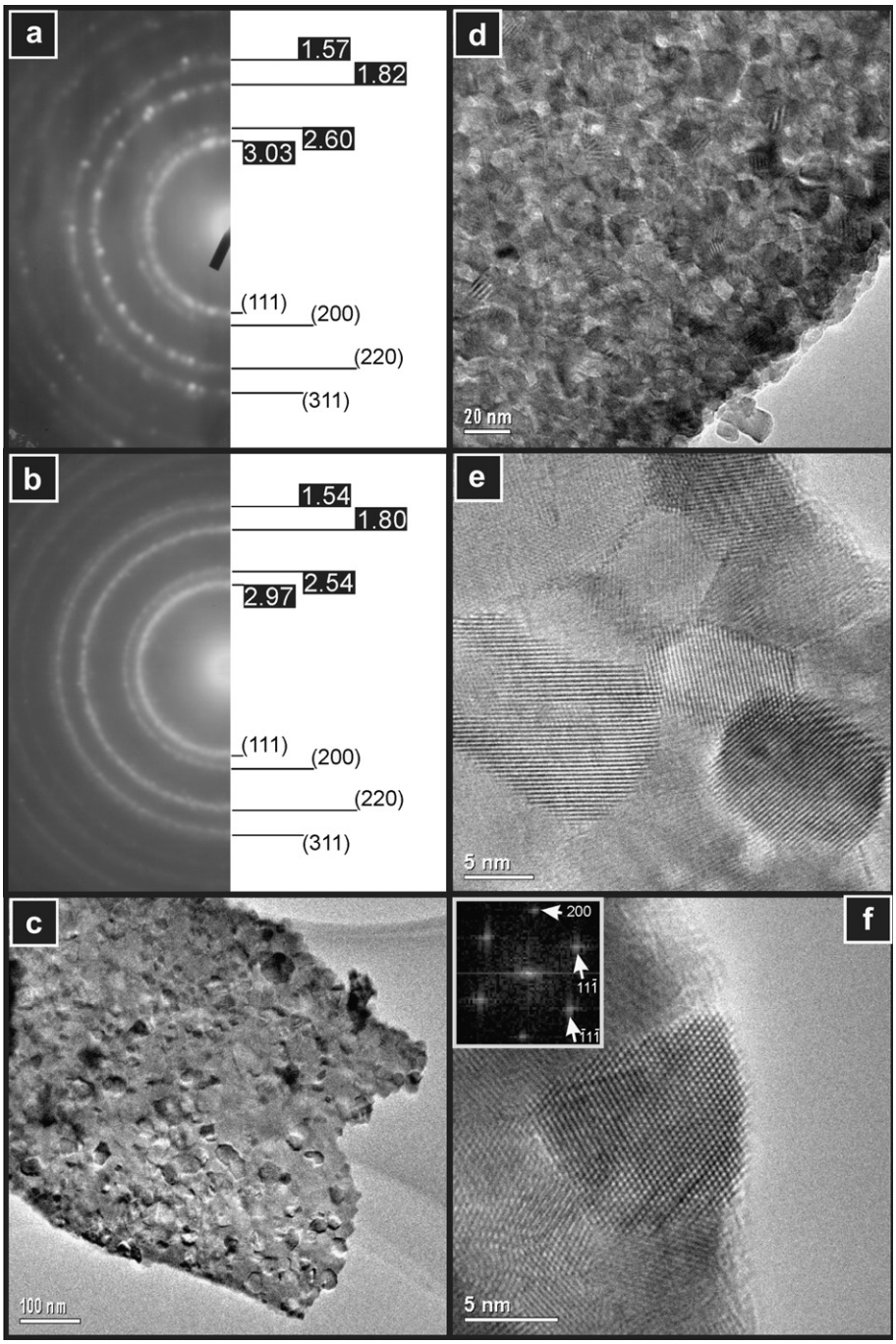

Fig. 4 – TEM diffraction patterns and images for samples prepared by the cation complexation method. SAEDs for (a) GDC10-CC; (b) GDC20-CC. Low magnification images for (c) GDC10-CC; (d) GDC20-CC. High resolution images for (e) GDC10-CC; (f) GDC20-CC, including DDP (inset) of the particle in the image indexed to the [011] zone axis of the fluorite structure and with Miller indices shown.

magnetic stirring. During the addition, successive color changes were observed (from yellow to light red, then light brown and finally violet) until a light violet-gray solid appeared, at a pH above 10. This suspension (where the microemulsion has not destabilized) was aged for 12 h. During this time, the suspension color turned light yellow, the characteristic color of ceria.

The next step involved the addition of ethanol to destabilize the microemulsion. The solid obtained was washed and centrifuged several times with additional ethanol to eliminate any remaining surfactant and/or organic residues (each time, the supernatant liquid was discarded). The washed solid was dried in a furnace at 125 °C, and heated in an oven at 600 °C for 1 h in air.

2.1.3. Template-filling method (TF)

Templates consisting of porous polycarbonate films were used as filters in an appropriate syringe filtration system to ensure that the total volume of the pores was filled with the cation nitrate precursor solution. The polycarbonate (PC) films used were commercially-available Isopore™ membrane filters from Millipore. Films with 800 nm pore pass diameters were used. The reaction to obtain the desired compound proceeded by the dehydration and denitrification of the confined precursor in a commercial microwave oven. For all compositions, an output power of 800 W was applied for 3 min. The desired compound was finally obtained and the template was burnt off in a standard furnace employing a thermal treatment in which the final step involved heating at 650 °C for 10 min in air. After this treatment, the furnace was allowed to cool freely to room temperature. The resulting material was a collection of tubular nanostructures whose diameters depended on the size of the pores of the template [14].

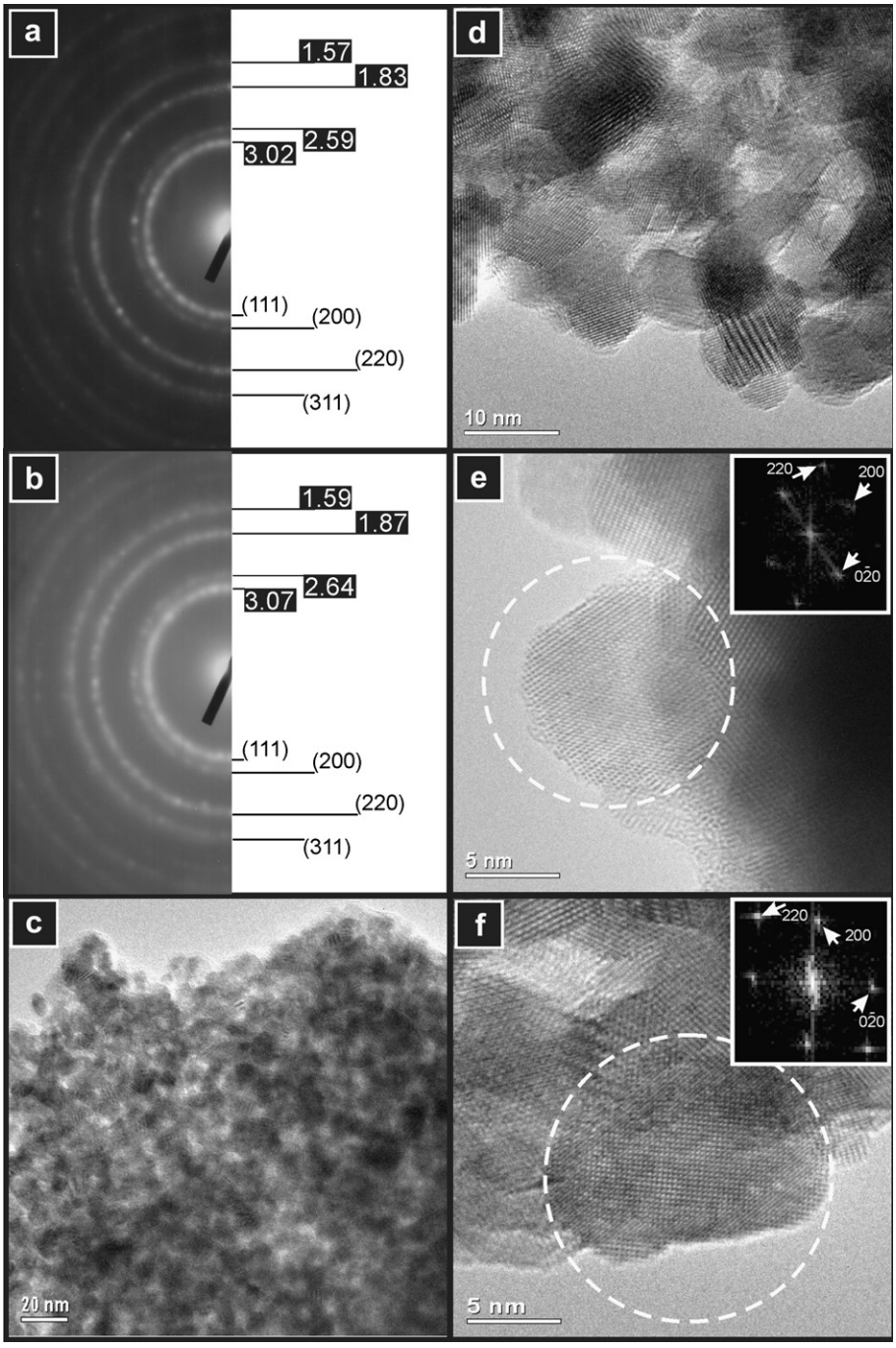

Fig. 5 – TEM diffraction patterns and images for samples prepared by the reverse microemulsion method. SAEDs for (a) GDC10-RM; (b) GDC20-RM. (c) Low magnification image for GDC10-RM; (d) Intermediate magnification image for GDC20-RM. High resolution images for (e) GDC10-RM; (f) GDC20-RM, both including DDPs (inset) of the particles circled and both indexed to the [001] zone axis of the fluorite structure with Miller indices shown.

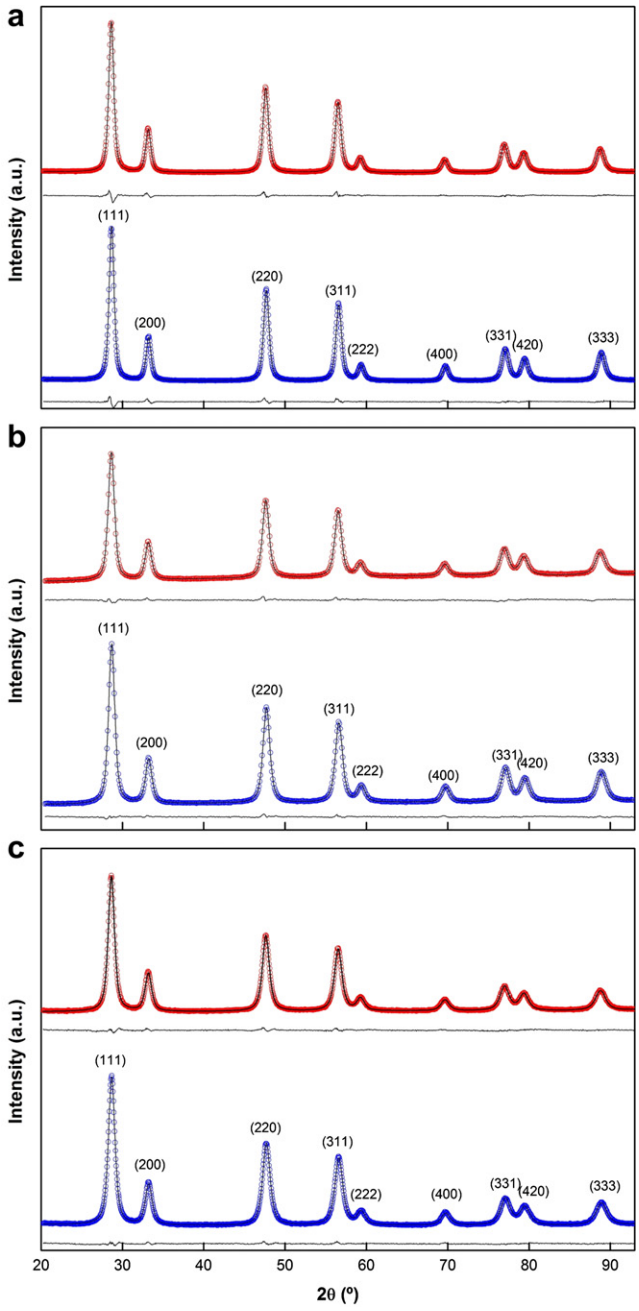

Fig. 6 – SR-XRD of (a) GDC10-CC (blue) and GDC20-CC (red); (b) GDC10-RM (blue) and GDC20-RM (red); and (c) GDC10-TF (blue) and GDC20-TF (red). All plots include the Rietveld-fitted pattern (black line) and the difference plot. (For interpretation of the references to color in this figure legend, the reader is referred to the web version of this article.)

2.2. *Physico-chemical characterization*

2.2.1. *Electron microscopy*

SEM images were obtained using a Philips XL30 E-SEM instrument which was fitted with a field emission gun. TEM images of the nanotube sample were obtained using a JEOL 2010 TEM instrument. This was equipped with a LaB_6 filament and a Gatan digital camera and was operated at 200 keV. The microscope also benefited from a system for performing Energy Dispersive X-ray Spectroscopy (EDS) and this was used to analyze the chemical compositions of the samples. For TEM study, samples were prepared by dipping a 3 mm copper grid coated with holey carbon film into a dispersion of the sample powder in acetone.

2.2.2. *Synchrotron X-ray diffraction*

Synchrotron XRD experiments were carried out using the D10B-XPD beamline of the LNLS (Brazilian Synchrotron Light Laboratory, Campinas, Brazil) in static air. A high-intensity (low-resolution) configuration, without a crystal analyzer, was employed. The wavelength was set at 1.5500(4) Å. Data in the angular region of $2\theta = 20 - 100^{\circ}$ were collected at room temperature in a step-scanning mode, with a step length of 0.05° and a step-counting time of 3 s. NIST SRM 640c Si powder was used as the standard for the instrumental broadening correction.

2.2.3. *Nitrogen adsorption-desorption measurements*

Specific surface area (SSA) measurements were carried out using Brunauer-Emmett-Teller (BET) absorption isotherm analysis by nitrogen adsorption-desorption (Autosorb-1, Quantachrome). The analysis of the isotherms provided the BET specific surface area. Outgassing was carried out at 300 °C for 4 h.

2.2.4. *Ce L_3-edge XANES*

In order to determine qualitatively the oxidation state of Ce in the GDC samples, XANES (X-ray absorption near-edge structure) spectra were collected at the D04B-XAFS1 beamline at LNLS in transmission mode using a Si(111) monochromator for the Ce L_3-edge. The nominal photon flux of the beamline is 3×10^9 photons/(s.mrad.100 mA)@6 keV. All spectra were collected at room temperature for energies in the range 5690–5780 eV using steps of 2 eV for 5690–5710 eV and 0.2 eV for 5710–5780 eV, with $E/\Delta E = 5000–10{,}000$. Energy was calibrated using a Cr foil. Several acquisitions (around 4 spectra) were carried out on the same sample to improve the signal to noise ratio.

2.2.5. *Preliminary catalytic tests*

Catalytic studies on GDC10-RM, GDC10-CC and GDC10-TF samples were performed in a fixed-bed flow reactor (quartz tube of 4 mm internal diameter, 60 cm length), operated isothermally at atmospheric pressure. The reactor was placed in an electric tubular oven equipped with a temperature controller. A thermocouple was placed axially into the quartz tube, directly into the sample as a way to provide an accurate temperature measurement. The sample (45 mg) was diluted with ground quartz wool in order to ensure an adequate contact with the reactants. The reactants were a mixture of methane (1.4 $cm^3\ min^{-1}$) and air (38.5 $cm^3\ min^{-1}$), with nitrogen added to the mixture to provide a total gas flow of 50 $cm^3\ min^{-1}$. In order to determine the extent of non-catalytic combustion of CH_4 in the reactor a blank run was performed using a fixed bed composed of only 400 mg of SiO_2. Measurements were performed in the 300–900 °C temperature range, at 50 °C increments. Several measurements were

taken at each temperature until the system reached steady state. Gas analysis were performed using a Perkin Elmer Clarus 500 gas chromatograph equipped with a thermal conductivity detector, an Altech CTR1 packed column, and using He as the carrier gas. Moisture was removed from the gases using a desiccant trap prior to injection into the chromatograph.

3. Results and discussion

3.1. Physico-chemical characterization

SEM images of GDC10-CC and GDC20-CC powders are presented in Fig. 2a and b, respectively. Both powders showed the typical morphology of GDC mixed oxides synthesized by the citrate complexation route, consisting of sheets in an egg shell-like structure. There is a large difference between the morphologies of these powders and those obtained by the reverse microemulsion method (Fig. 3c and d). In the case of GDC10-RM and GDC20-RM, the aggregates are characterized by an angular shape. In both cases, there is a high degree of agglomeration.

For GDC synthesized by the template-filling method, tubular morphology was observed. The SEM images of GDC10-TF and GDC20-TF are shown in Fig. 3a and b,c and d, respectively. Fig. 3 shows a large cluster of tubular structures and illustrates the very high yield of these structures obtained. Individual tubes showed consistent geometries, especially in terms of their diameters, which were typically between 500 and 600 nm. Tube lengths varied more than diameter, falling into the range from 1 to 5 μm. No significant differences were observed between the dimensions of the two different compositions.

Diffraction patterns and images obtained in the TEM for the samples prepared by the cation complexation (CC) and reverse microemulsion (RM) methods are presented in Figs. 4 and 5, respectively. Comparable information for the nanostructured tubular GDC materials made using the template-filling (TF) method is available elsewhere [14]. Selected Area Electron Diffraction patterns (SAEDs) were recorded for all six samples from areas containing a large number of particles (Figs. 4 and 5a and b and Figs. 7 and 8a in [14]). These patterns could be indexed to the cubic Fluorite structure in all cases. The concentric rings in all of the SAEDs imply diffraction from a large number of small crystallites aligned in all possible orientations. In low to intermediate magnification images, these crystallites are seen to form sheets in the CC samples, similar sheets which curve around to form tubes in the TF samples and thicker agglomerations in the RM samples. The primary particles are generally quite rounded in shape, with many surface facets, and the majority in each sample falls into the size range 5–15 nm. In the CC samples, there is a tendency towards slightly larger and more angular primary particles and in some images these appear to lock together like grains within the thin sheets already mentioned (Fig. 4e). Again, for all samples, the high resolution images clearly show the internal crystal lattice structure confirming the high crystallinity of the nanoparticles of which these materials consist. Digital Diffraction Patterns (DDPs) were obtained by performing Fourier transforms on the images of such particles and examples are given as insets in Figs. 4 and 5 and in [14]. These patterns were successfully indexed to the Fluorite structure viewed along either the [001] or [011] zone axis. The Miller indices corresponding to the spots in the DDPs are indicated in the figures.

EDS spectra were obtained from a number of regions of each sample and the relative quantities of Gd and Ce were extracted. EDS analysis for the TF method is given in [14]. Molar ratios of Gd to total cations (Gd + Ce) for GDC10-CC, GDC20-CC, GDC10-RM and GDC20-RM of 0.112, 0.208, 0.102 and 0.206, respectively, were obtained. These are close to the values of 0.1 and 0.2 expected.

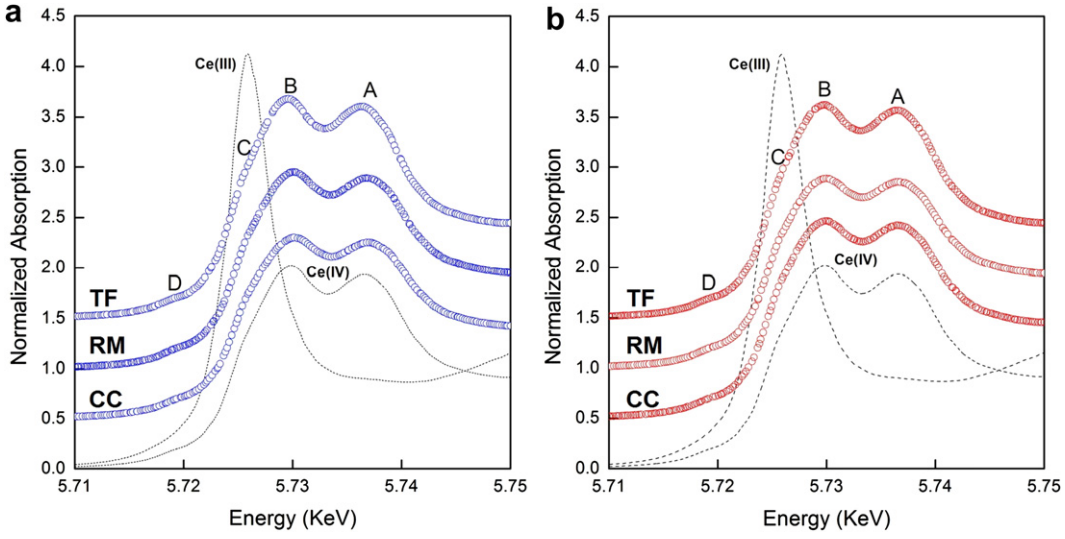

Fig. 7 – Ce L_3-edge XANES normalized absorption spectra for (a) GDC10 and (b) GDC20. Reference standards of micrometric (dashed line) CeO_2 - for Ce(IV) - and $Ce(NO_3)_3$ (full line) – for Ce(III) - are included. Four characteristic peaks of XANES spectra for CeO_2 are indicated by capital letters.

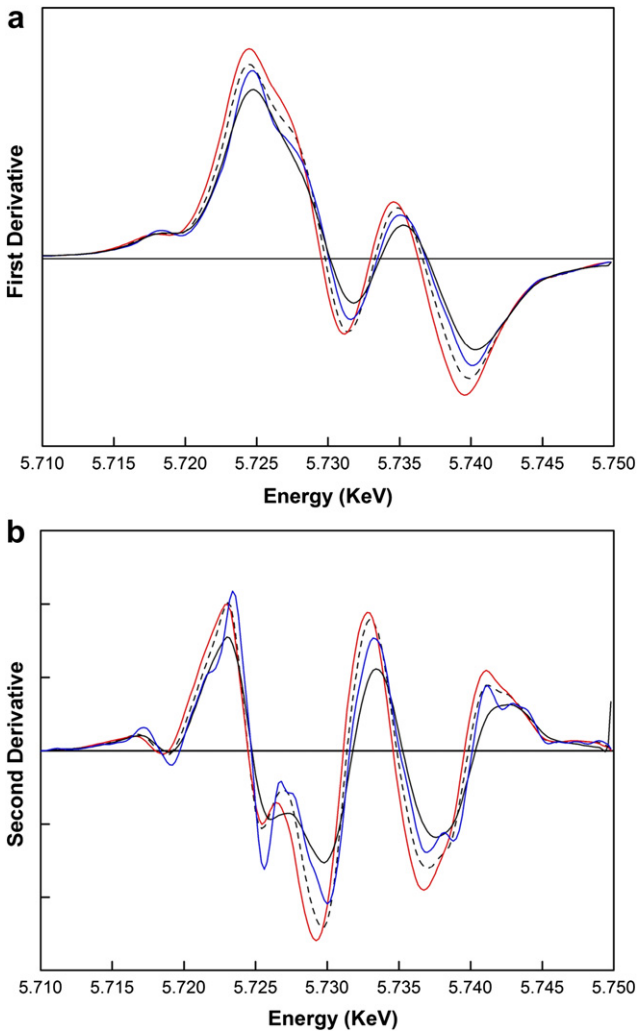

Fig. 8 – a) First and (b) second derivatives of Ce L_3-edge XANES normalized absorption spectra for micro-CeO_2 (dashed line), GDC10-CC (black line), GDC10-RM (blue line) and GDC10-TF (red line). (For interpretation of the references to color in this figure legend, the reader is referred to the web version of this article.)

A crystallographic study was performed by Rietveld refinement of the SR-XRD data employing the FullProf suite of software [17]. For the cubic phase, the *Fm3m* space group was assumed, with (Gd^{3+}, Ce^{4+}) cations and O^{2-} anions in 4a and 8c positions, respectively. The peak shape was assumed to be a pseudo-Voigt function. The background of each profile was fitted using a six-parameter polynomial function in $(2\theta)^n$, $n = 0–5$. The thermal parameters were assumed to be equal. In Fig. 6a–c, SR-XRD patterns recorded at room temperature for the nanostructured GDC10 and GDC20 samples, the Rietveld-fitted pattern (line) and the difference plot are exhibited. The results of Rietveld refinements of the SR-XRD data for the nanostructured samples are summarized in Table 1. In this table, the refinements are accompanied by reliability indices to judge the fitting quality. These indices are weighted R (R_{wp}), the reduced chi-squared (χ^2), and R_e, which are related just to the profile of the XRD patterns, and R_p, which is related to the crystal structure. The reduced chi-squared is defined by $(R_{wp}/R_e)^2$, where R_{wp} is the index that should be analyzed to verify if the refinement is converging and R_e is the expected statistical value for R_{wp}.

All GDC compositions exhibited a cubic structure (*Fm3m* space group) and the lattice parameters showed a cell expansion with increasing Gd content. In GDC solid solutions, a unit cell expansion is expected to occur because of the replacement of Ce^{4+} (0.97 Å) by Gd^{3+} (1.02 Å). The estimated lattice parameters for both compositions are in good agreement with JCPDS entries no. 75–0161 and no. 75–0162.

In figure Fig. 6, all SR-XRD patterns exhibited resolvable peaks but with relatively severe line broadening. This broadening was ascribable to the presence of small crystallites. The average crystallite size, D_{XRD}, was determined using the Scherrer formula [18], at the peak position of the main reflection (111). Errors in crystallite size were derived by estimating the error in the FWHM (full-width at half-maximum) to be equal to the 2θ step.

All samples exhibited a small average crystallite size (Table 1). Nanostructured GDC powders obtained using the cation complexation method exhibited larger crystallite sizes than the other GDC samples.

In Table 2, SSA and the primary particle size, d_{BET}, calculated from the BET data, are summarized. It can be seen that the GDC10-FT and GDC10-RM showed the highest values of SSA (97 $m^2\ g^{-1}$ and 77 $m^2\ g^{-1}$, respectively), while the lowest values were obtained for GDC20-CC (23.4 $m^2\ g^{-1}$). The d_{BET}/D_{XRD} ratio in the GDC10-FT and GDC10-RM samples were about 1.3 and 1.7, respectively, indicating that the crystallites in both samples exhibited a low degree of agglomeration. On this measure, the materials synthesized using the citrate complexation route showed significantly more agglomeration.

In Fig. 7, the Ce L_3-edge XANES spectra of the GDC10 (Fig. 7a) and GDC20 (Fig. 7b) samples are compared with that of the CeO_2 reference and with cerium (III) nitrate. The Ce L_{III}-edge is frequently used as a "fingerprint" to characterize the electronic properties of ceria-based materials. However, the electronic transitions behind these XANES features are complex and not fully understood. In pure CeO_2, the Ce L_{III}-edge exhibits two clear peaks frequently labeled A and B. Peak A is a Ce^{4+} peak with the final state of $2p4f^05\ d^1$, which denotes that an electron is excited from the Ce 2p shell to its 5d shell,

Table 1 – Structural parameters, standard Rietveld agreement factors and crystallite average size (D_{XRD}) for GDC10 and 20 obtained by cation complexation (CC), reverse microemulsion (RM) and template-filled (TF) methods.

Sample	a/Å	R_p	R_{wp}	R_e	χ^2	D_{XRD}/nm
GDC10-CC	5.4210(6)	4.41	5.74	3.22	3.18	13.2(8)
GDC20-CC	5.4283(6)	5.01	6.31	3.33	3.59	12.9(7)
GDC10-RM	5.4193(5)	3.09	2.86	1.71	2.78	10.2(5)
GDC20-RM	5.4274(5)	5.15	4.41	2.04	4.69	10.2(5)
GDC10-TF	5.4202(6)	3.93	3.60	2.12	2.87	9.6(4)
GDC20-TF	5.4267(4)	4.61	4.06	2.35	2.98	9.9(4)

Table 2 – Specific surface area (SSA) and calculated primary particle size (d_{BET}) for GDC10 and 20 obtained by cation complexation (CC), reverse microemulsion (RM) and template-filled (TF) methods.

Sample	SSA/m^2 g^{-1}	d_{BET}/nm	d_{BET}/D_{XRD}
GDC10-CC	29.0(5)	33.2	2.52
GDC20-CC	23.4(7)	41.2	3.20
GDC10-RM	77.2(4)	12.5	1.22
GDC20-RM	50.6(6)	19.0	1.86
GDC10-TF	97.0(5)	9.9	1.04
GDC20-TF	61.2(3)	15.7	1.58

with no electron in the 4f shell. Peak B is also a Ce^{4+} peak, with the final state of $2p4f^15d^1v$, which denotes that in addition to an electron excited from the Ce 2p shell to the 5d shell, another electron is also excited from the valence band (O 2p shell) to the Ce 4f shell, leaving a hole (v) in the valence band. Some authors refer to Peak C as a Ce^{3+} peak [19]. An additional small peak (D) is present at pre-edge and likely arises from transitions to the bottom of the conduction band.

In Fig. 7 two main peaks (labeled A and B) separated by approximately 7 eV are observed in the CeO_2 spectrum. These two features were also detected for all other samples, with an intensity ratio close to that found in the CeO_2 sample. Although the presence of Ce^{3+} ions in the GDC samples cannot be completely excluded, based on the comparison with the reference compound, the Ce atoms appear to be mainly in the tetravalent state. In fact, the small shoulder corresponding to Peak C in these spectra is consistent with the expected increase in the fraction of Ce ions in low coordination environments at the surface of these high surface area nanostructured materials, i.e. because of surface to volume effects.

First and second derivatives of the Ce L_3-edge XANES spectra for nanostructured GDC10 and GDC20 are exhibited in Figs. 8 and 9, respectively. According to the second derivative, the Ce L_3-absorption edges for all samples are close to 5724.5 eV.

3.2. *Preliminary catalytic test for CH_4 combustion*

In order to obtain an indication of the catalytic activity of nanostructured materials, several tests were performed on the GDC10 materials, as explained in the experimental section. The GDC10 compositions were chosen for catalytic evaluation because they exhibited larger SSAs than the GDC20 materials. In order to allow a comparison between samples of the same composition but different morphologies, samples of GDC10-TF, GDC10-RM and GDC10-CC were tested, thus providing a sample with high SSA (97 m^2 g^{-1}) and one with a typical medium-to-low SSA (29 m^2 g^{-1}), respectively.

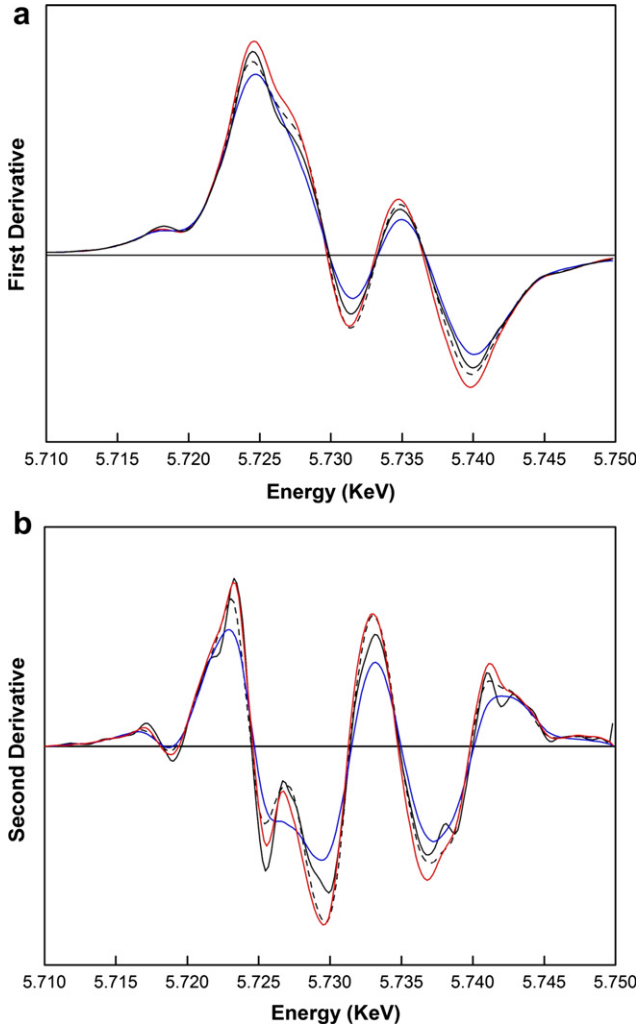

Fig. 9 – a) First and (b) second derivatives of Ce L_3-edge XANES normalized absorption spectra for micro-CeO_2 (dashed line), GDC20-CC (black line), GDC20-RM (blue line) and GDC20-TF (red line). (For interpretation of the references to colour in this figure legend, the reader is referred to the web version of this article.)

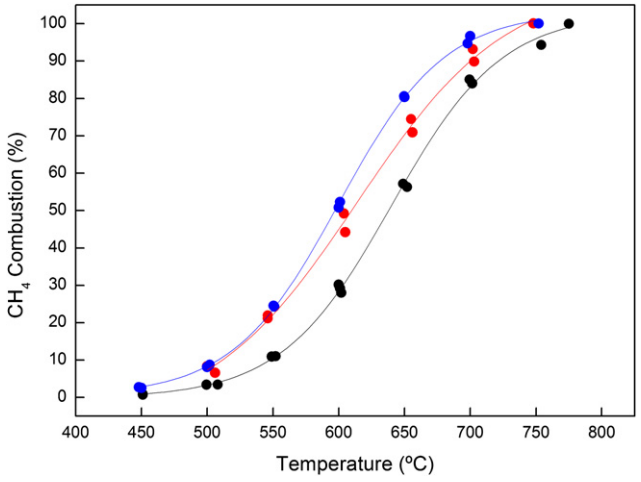

Fig. 10 – Catalytic results of CH_4 combustion for GDC10-CC (black circles), GDC10-RM (red circles) and GDC10-FT (blue circles) samples at different temperatures. (For interpretation of the references to colour in this figure legend, the reader is referred to the web version of this article.)

In Fig. 10, CH_4 conversion versus temperature for different catalyst samples are plotted. The temperature at which 50% of CH_4 conversion was reached (T_{50}) was used as an index of catalytic activity. T_{50} values were estimated from the experimental curves [20]. The non-catalytic sample (blank test) exhibited the highest value of T_{50} (883 °C), GDC10-CC and GDC10-RM gave values of 638 °C and 610 °C, respectively. The tubular GDC10-TF sample exhibited the lowest value of T_{50} (597 °C) and, therefore, appeared to be the most active catalyst under these conditions. Clearly, the increase in SSA seems to be responsible for the enhanced catalytic activity of GDC10-TF.

4. Conclusions

In the present work, we report on the preparation of CeO_2–Gd_2O_3 mixed oxide employing three different chemical methods. The resulting nanostructures were characterized by employing synchrotron radiation X-ray diffraction, XANES, SEM and HRTEM and EDS.

All nanostructured mixed oxides were found to have a cubic crystal phase (*Fm3m* space group) with average crystallite sizes ranging from 9.6 to 13.2 nm. Tubular nanostructured GDC10 obtained using a template-filling method exhibited the largest specific surface area while the lowest values were obtained from the cation complexation method.

XANES results indicated that the Ce^{4+} state is in the majority, although a small amount of the Ce^{3+} state was detected.

Preliminary catalytic studies showed that tubular nanostructured GDC10 samples exhibited an improved catalytic activity towards CH_4 oxidation compared to the GDC10 nanopowders. These findings open up an interesting avenue for future work in this area, and indicate a promising possible application for this particular system.

Acknowledgments

This work has been supported by: the Brazilian Synchrotron Light Laboratory (LNLS, Brazil), under proposals D10B-XPD-8572, D04B-XAFS1-8175 and D04B - XAFS1-9218; the Agencia Nacional de Promoción Científica y Tecnológica (Argentina, PICT No. 38309); PIDDEF No. 0022/08/CITEDEF and the Latin American Centre of Physics (CLAF). The TEM was performed at the Electron Microscopy Facility, University of St Andrews. Special thanks to M. Cabezas and Dr. S. Larrondo for useful discussions regarding the catalytic tests. Dr. R.O. Fuentes is member of CIC-CONICET, Argentina.

REFERENCES

[1] Steele BHC. Appraisal of $Ce_{1-y}Gd_yO_{2-y/2}$ electrolytes for IT-SOFC operation at 500 °C. Solid State Ionics 2000;129:95–115.
[2] Kilner J. Fast oxygen transport in acceptor doped oxides. Solid State Ionics 2000;123:13–23.
[3] Steele BHC. Running on natural gas. Nature 1999;400:619–21.
[4] Park S, Vohs J, Gorte R. Direct oxidation of hydrocarbons in a solid-oxide fuel cell. Nature 2000;404:265–7.
[5] Ivanov VV, Khrustov VR, Kotov Yu A, Medvedev AI, Murzakaev AM, Shkerin SN, et al. Conductivity and structure features of $Ce_{1\_x}Gd_xO_{2\_d}$ solid electrolytes fabricated by compaction and sintering of weakly agglomerated nanopowders. J Eur Ceram Soc 2007;27:1041–6.
[6] Yu T, Joo J, Park YI, Hyeon T. Large-scale nonhydrolytic sol–gel synthesis of uniform-sized ceria nanocrystals with spherical, wire, and tadpole shapes. Angew Chem Int Ed 2005;44:7411–4.
[7] Zhang TS, Ma J, Kong LB, Hing P, Leng YJ, Chan SH, et al. Sinterability and ionic conductivity of coprecipitated $Ce_{0.8}Gd_{0.2}O_{2\_d}$ powders treated via a high-energy ball-milling process. J Power Sources 2003;124:26–33.
[8] Rocha RA, Muccillo ENS. Physical and chemical properties of nanosized powders of gadolinia-doped ceria prepared by the cation complexation technique. Mater Res Bull 2003;38(15):1979–86.
[9] Yaremchenko AA, Valente AA, Kharton VV, Bashmakov IA, Rocha J, Marques FMB. Direct oxidation of dry methane on nanocrystalline Ce0.8Gd 0.2O2−δ/Pt anodes. Catal Commun 2003;4:477–83.
[10] Jiang SP, Chen XJ, Chan SH, Kwok JT. GDC-impregnated $(La_{0.75}Sr_{0.25})(Cr_{0.5}Mn_{0.5})O_3$ anodes for direct utilization of methane in solid oxide fuel cells. J Electrochem Soc 2006;153(5):A850–6.
[11] Hennings U, Reimert R. Noble metal catalysts supported on gadolinium doped ceria used for natural gas reforming in fuel cell applications. Appl Catal B 2007;70:498–508.
[12] Jadhav LD, Chourashiya MG, Subhedar KM, Tyagi AK, Patil JY. Synthesis of nanocrystalline Gd doped ceria by combustion technique. J Alloys Compd 2009;470:383–6.
[13] Fuentes RO, Acuña LM, Zimicz MG, Lamas DG, Sacanell J, Leyva AG, et al. Formation and structural properties of Ce–Zr mixed oxide nanotubes. Chem Mater 2008;20(23):7356–63.
[14] Fuentes RO, Muñoz FF, Acuña LM, Leyva AG, Baker RT. Preparation and characterisation of nanostructured gadolinia-doped ceria tubes. J Mater Chem 2008;18:5689–95.
[15] Fuentes RO, Baker RT. Synthesis and properties of gadolinium-doped ceria solid solutions for IT-SOFC electrolytes. Int J Hydrogen Energy 2008;33:3080–4.
[16] Fuentes RO, Baker RT. Structural, morphological and electric properties of $Gd_{0.1}Ce_{0.9}O_{1.95}$ prepared by a citrate complexation method. J Power Sources 2009;186(2):268–77.
[17] Rodríguez-Carvajal J. FullProf98, Version 0.2. Laboratoire León Brillouin. Saclay, France: CEA-CNRS; 1998.
[18] Klug H, Alexander L. X-ray diffraction procedures for polycrystalline and amorphous materials. New York: John Wiley; 1974. p. 618.
[19] Zhang F, Wang P, Koberstein J, Khalid S, Chan S- W. Cerium oxidation state in ceria nanoparticles studied with X-ray photoelectron spectroscopy and absorption near edge spectroscopy. Surf Sci 2004;563:74–82.
[20] Specchia S, Conti F, Specchia V. Kinetic studies on Pd/$Ce_xZr_{1-x}O_2$ catalyst for methane combustion. Ind Eng Chem Res 2010;49:11101–11.